Extending the Capabilities of Rainfall Estimation from Satellite Infrared via a Long-Range Lightning Network Observations

Carlos A. Morales* and Emmanouil N. Anagnostou

Department of Civil and Environmental Engineering

University of Connecticut,

Storrs, Connecticut

Current affiliation: Department of Meteorology,

University of Sao Paolo, Brazil

Submitted to *Journal of Hydrometeorology*

Revised manuscript submitted: April 2002

Accepted: May 2002
Corresponding author: Emmanouil N. Anagnostou, (860) 486-6806, manos@engr.uconn.edu

Abstract

An algorithm for real-time precipitation estimation that combines satellite infrared with long-range lightning network observations is developed. The emphasis is made on enhancing current capabilities into continuous rainfall monitoring over large regions at high spatio-temporal resolutions and in separating precipitation type in its convective and stratiform components. Lightning information is retrieved from an experimental long-range Very Low Frequency radio receiver network named Sferics Timing and Ranging Network (STARNET). Parameterizations for delineating the total rain area and its convective portion as well as convective and stratiform rain rate relationships are obtained for lightning (LTG) and lightning-free (NLTG) clouds. The procedure accounts for differences in land versus ocean and for various levels of cloud system maturity. The parameters are evaluated using as reference the most definitive precipitation fields and rain classification estimates derived from the Tropical Rainfall Measuring Mission (TRMM) Precipitation Radar (PR). The algorithm is evaluated based on independent PR estimates and measurements from a rain gauge network in Florida. Overall, the algorithm underestimates rain area with respect to PR for LTG and NLTG clouds by about 20%, while for the rain volume there is an overestimation of ~19% for LTG and ~12% for NLTG clouds. Comparison of hourly estimates with rain gauges revealed an overall overestimation of 6% at 0.1 degree scale. At monthly scales, the biases are 2.4% and 0.27% for 1-and 2-degree resolutions. The significance of lightning information on rainfall estimation accuracy is investigated by applying the proposed technique without lightning information. Comparisons with the PR showed that in rain area determination there is an overall bias reduction of 31% by using lightning information. In rain gauge comparisons, the bias reduction from incorporating lightning data is 87% for the hourly

0.1-degree estimates. In regards to correlation, the increase in hourly estimates varies from 0.13 to 0.03 for scales ranging from 0.1 to 1 degree.

1. Introduction

Information on the spatial and temporal variability of global precipitation is of fundamental importance to applications ranging from hydrologic engineering to climate change research. This paper presents an algorithm developed for continuous (in time) retrieval of instantaneous surface rainfall over a large region containing North and South America and part of the Atlantic and Pacific Oceans using information from an experimental long-range lightning detection network, geo-stationary satellite infrared observations, and adjacent rainfall measurements from the first space-borne precipitation radar (PR) onboard the Tropical Rainfall Measuring Mission (TRMM) satellite (Simpson et al. 1996). This study is formulated under the hypotheses that: (1) lightning is correlated with the presence of precipitation sized ice particles that are associated with deep convective cores: this observation can improve the identification of convective rain area; (2) the precipitation area and its convective portion are related to the cloud and lightning areas of a precipitating system; and (3) lightning and lightning free clouds exhibit different precipitation characteristics.

We use a fairly new technology on the continuous detection of lightning occurrence over very large areas (several millions of square kilometers), which is based on a network of very low frequency (VLF) radio receivers. This indirect rainfall information in conjunction with other space-based remote sensing data could be used to improve the global rainfall monitoring at finer spatial (< 25×25 km) and temporal scales (< 1 hour). Baker et al. (1995) have shown that charge separation in thunderstorms is produced by non-inductive ice-ice interactions [1] at temperatures less than -10^{o}C and concentrations of super-cooled water in a critical range. Updraft velocities within the electrified precipitating clouds must be sufficiently intense to create an adequate

differential velocity between dense negatively charged, large ice particles and smaller, positively charged ice-ice interaction[2] particles. This charge separation gives rise to lightning discharges, which may take place between cloud and ground (CG) or, more frequently and earlier in the development of the thunderstorms as intra-cloud (IC) lightning. These electrical discharges emit radio noise (i.e., sferics) that can be measured continuously at large distances (thousands of kilometers) by VLF radio receivers (see for more detailed discussion Lee, 1986, Cramer and Cummins, 1999; and Morales, 2002a). An experimental network of five ground-based radio receivers situated along the United States east coast and Puerto Rico (see Figure 1), named Sferics Timing and Ranging Network (STARNET), has measured sferics between July 1997 and February 1998 (Morales et al., 2002a).

The relation of lightning to precipitation has been the subject of various precipitation remote sensing and climatology studies. Workman and Reynold (1949) related flash rates to convective rain fluxes, and suggested that the frequency of lightning may be a measure of convective activity. Goodman (1990) developed a relationship between lightning frequency and rainfall intensity for systems in Florida. Similarly, Buechler et al. (1994) demonstrated a linear relationship between rainfall and lightning activity for Florida thunderstorms and Tappia et al. (1998) estimated convective rainfall rate from rainfall-lightning ratios using the Melbourne, Florida, WSR-88D radar. Petersen and Rutledge (1996, 1998), in a more generalized study computed ratios of rainfall yields to cloud-to-ground lightning flash frequency for different parts of the world and found dependency on environmental regimes.

Satellite infrared (IR) images have been used to retrieve rainfall at large spatial and temporal scales, and for delineation of rain areas in cloud systems (Arkin, 1979, and Arkin and

[1] Ice-ice interactions is the process of collision between ice particles;

Meisner, 1987). Adler and Negri (1988) developed a technique to distinguish convective and stratiform precipitating systems based on the temperature gradients evaluated around the minimum temperature in the cloud clusters. Recently, Vicente et al. (1998) presented an auto-estimator IR technique that uses additional information of precipitable water and relative humidity from a numerical weather prediction model. They produce their best hourly estimates at larger grids (48x48 km or larger) and exaggerate the rain areas. These IR rainfall estimation methods have deficiencies associated with the presence of thin non-precipitating cirrus clouds and non-raining cold Mesoscale Convective System (MCS) cloud shields. Anagnostou et al. (1999a) in an effort to minimize this uncertainty used a statistically adjusted IR technique with microwave sensors and showed that the area within a cloud cluster whose temperature is at or below the most frequent temperature in that cluster is well-correlated with rain area. They were also able to improve the convective and stratiform rain area delineation in those precipitating systems. Despite those efforts on improving IR algorithms, there is considerable uncertainty in the estimates since the relation between cloud-top longwave IR brightness temperature and the underlying surface rainfall is complex and is based on indirect physical relationships.

Morales et al. (1997) have shown that lightning measurements associated with active convection in the clouds can provide reliable delineation of the convective cores, which would lead to improvements in the convective rain estimation. Grecu et al. (2000) used a combination of lightning and IR brightness temperatures to retrieve rainfall for a 15-day summer period over the United States. They showed that this combination could reduce by 15% the error variance of rain volume estimates compared to an IR only scheme for clouds associated with lightning. The

[2] Positive charge ice-ice interaction is the effect of charge transfer between denser ice particles (hail, graupel, snow pellet) negatively charged falling over cold air that has small ice particles positively charged;

authors also demonstrated that lightning information could improve the overall rainfall estimation accuracy compared to an IR only approach.

This paper presents a lightning-IR-rainfall algorithm that consists of procedures for estimating rain area and its convective/stratiform portions for clouds with lightning (LTG) and lightning free (NLTG). Convective and stratiform rainfall rates are related to lightning rates and IR brightness temperatures through relationships determined using the TRMM PR precipitation products as reference. Evaluation of the algorithm (defined as the Sferics Infrared Rainfall Technique, SIRT) performance based on an independent set of PR rain estimates and a gauge network measurements is performed, and the significance of lightning information on rainfall retrieval accuracy is investigated. Discussion of future investigations is offered in our conclusions.

2. Algorithm development

The main hypotheses inherent in this algorithm development are that: (1) lightning information can advance our ability to discriminate convective rain areas within a cloud system, given that current IR algorithms face limitations in dealing with the presence of cirrus clouds and non-raining cloud shields like those in MCS; and (2) the development of a combined lightning and satellite IR algorithm based on the newly available PR rain products can lead to improvements in the definition of rain area, precipitation classification, and quantitative rain estimation from these sensors. The algorithm is designed to produce maps of instantaneous surface rainfall fluxes and rain type classification based on a combination of lightning measurements from STARNET, IR brightness temperature (10.2-11.2 μm) observations, and

precipitation profile measurements from PR. The objective is to retrieve rain area and rates that are statistically consistent with the rain fields derived from PR observations.

The lightning information used here is based on an experimental long-range lightning detection network (Morales et al., 2002a). The network uses five radio receivers in the very low frequency (VLF) spectrum between 5 and 15 kHz (centered at 9.8 kHz). Each receiver measures the vertical electric field and includes a time stamp synchronized to a GPS clock (with one microsecond accuracy). These electric field time series represent sferics waveforms of a lightning source that propagates through the ionosphere-Earth wave-guide. The time correlation between any two-station waveforms defines an arrival time difference (ATD), which represents locations with same time difference between the two stations. Those locations define hyperbolas over the earth's surface. The intersection of several ATDs (hyperbolas) from a sferics candidate defines a "lightning fix" location, which is identified numerically by minimizing a quadratic function of modeled and measured ATDs (Lee, 1986; Morales et al., 2002a). Figure 1 shows the network configuration that has receivers located in West Greenwich RI, Fairfax VA, Hunstville AL, Miami FL, and San Juan PR. A validation study by Morales et al. (2002a) has shown location errors reaching 60 km at very long distances (>4,000 km) from the vicinity of the network, while at ranges within 2,000 km errors are most likely to be below 15 km. Consequently, the precipitation estimation algorithm applies a spatial resolution of 0.1 x 0.1 degree, which accounts for the lightning location accuracy and the GOES-8 parallax effect. Another important issue is STARNET's CG lightning detection efficiency, which has been determined to be between 80% and 100% in the eastern United States and western Atlantic and dropping exponentially to 20% at distances beyond 4,000 km (Morales et al., 2002b). An empirically determined detection efficiency adjustment was applied to account for this range

effect in detection efficiency (DE) as discussed in Morales et al. (2002b). Figure 1 shows the STARNET DE as determined by Morales et al. (2002b). GOES infrared brightness temperature data were available at 30-minute time intervals and at full spatial resolution (field of view of 4 x 4 km at nadir). The data were compiled, calibrated, and navigated using the Man-computer Interactive Data Access System (McIDAS) data management software.

Precipitation fields and type classification products retrieved from TRMM science data and information system 2A-25 and 2A-23 algorithms (Awaka et al., 1997; Kummerow et al., 1998) are the reference rainfall data source used in this study. The PR products have 4.5 km horizontal and 250 m vertical resolution, but are limited to a PR swath of ~220 km that introduces considerable sampling issues. These issues are caused by the nature of the TRMM instantaneous measurements, which represent snap-shots of the current status of the observed precipitation. Since the proposed algorithm is calibrated against those products, it is expected that its retrievals would carry (in addition to any algorithm uncertainties) the potential PR rain estimation errors associated with attenuation correction and in the variability of the relationship between reflectivity (Z) to rainfall rate (R). Nevertheless, these rain estimates constitute the most comprehensive and advanced data set available for our algorithm development.

The study period and area used for algorithm development and evaluation consists of three months (December 1997 to February 1998) of coincident sensor data from 125W to 45W in longitude and 40N to 10S in latitude (an area of 4,000 square degrees). The period was selected due to its completeness in all data sets. The first two months (December 1997 and January 1998) of coincident STARNET, GOES, and TRMM-PR measurements are used to build the algorithm relationships. During this calibration period, we used a total of 631 TRMM-PR orbits coincident with IR and lightning measurements. In those orbits there were a total of 366 LTG and 3,103

NLTG clouds. Independent PR data from the February 1998 period is used for evaluating the algorithm's performance, which is presented in section 5.

The PR, GOES, and STARNET data were organized over the PR coverage within the common rectangular grid (125W-45W and 40N-10S) at 0.1-degree resolution grid cells. For each PR overpass, a grid cell was considered "cloudy" when the mean grid cell IR temperature was colder than 258 K. The data were collocated within ± 7.5 minutes of the GOES time (equator scanning crossing time). It is noted that 90% of the STARNET lightning fixes are within IR temperature less than 258 K. The cloud systems are separated to LTG versus NLTG and land versus ocean surfaces. This separation is necessary to account for the rain variability observed in the different types of raining systems and to achieve a better delineation of the convective rain areas. Figure 2 shows the convective and stratiform rainfall distribution as observed by PR for NLTG (black line) and LTG (red line) clouds at 0.1-degree resolution. These histograms indicate that LTG clouds produce higher rainfall rates in both rain types, which is in line with our expectation. The convective rainfall shows a broader distribution and stratiform with a longer tail in LTG clouds relative to NLTG clouds.

Rain type information based on TRMM-PR classification data offers three discrete rain classification types: stratiform, convective, and others (Awaka et al., 1997). A procedure is devised to aggregate PR classification estimates from the full resolution (4.5 km) to a lower resolution (0.1 degrees) used herein. Upon the inspection of their statistical rain distribution properties, two main categories are re-defined: stratiform and convective; where, the stratiform, other, and mix of stratiform/other rain pixel types are assigned to stratiform type; while the convective, and mix of convective/stratiform, convective/other, and convective/ stratiform/other types are assigned to convective type. The algorithm components are described next.

3. Assignment of Rain Areas

Within a cloud system (defined by a threshold brightness temperature of 258 K), delineation of the rainy area is a function of cloud type (LTG vs. NLTG), the most frequent IR temperature of the cloud (hereafter called T_{mode}), and the area (A_{Tmode}) within the T_{mode} isotherm. Separation of the data into several T_{mode} intervals prior to calibration has been observed by Anagnostou et al (1999) to produce better retrievals of rain area than using a single calibration for all of the data. After inspection of both LTG and NLTG clouds the following T_{mode} categories were defined as the most appropriate to delineate rain area. For the NLTG clouds the T_{mode} classes are defined at the following ranges: <215, 215-225, 225-235, 235-245, 245-250 and T_{mode} >250 K. For the LTG clouds the T_{mode} ranges are: <215, 215-220, 220-225, 225-230, 230-235, 235-240, 240-245, 245-250, and T_{mode} >250 K.

Figures 3a,b show the best-fit relationships between rainy area fraction (A_{rain}) and A_{Tmode} (both expressed as fractions of the total cloud area A_{cloud}) for NLTG and LTG clouds, respectively. It is apparent that for both cloud types, A_{rain} decreases relative to A_{Tmode} as clouds with higher T_{mode} values are considered. Comparison between ocean and land systems (not shown here) revealed that rain area fraction does not differentiate between land and ocean background. It is noted that at higher temperatures the rain area relationships tend to be linear. The NLTG clouds have less relative rainy area than LTG clouds, which is expected since in LTG clouds convection is deeper and associated with higher production of rainfall. Consequently, the rain area relationships are defined according to the following expressions:

$$A_{rain}(\%) = a+b(A_{Tmode}/A_{cloud}) \quad (1a)$$

$$A_{rain}(\%) = a(A_{Tmode}/A_{cloud})^{b}, \text{ for } T_{mode}<225 \text{ K \& NTLG clouds} \quad (1b)$$

The above relationships are evaluated separately for each cloud type (LTG vs. NLTG) and T_{mode} category as shown in Figure 3. Evaluation of these regression coefficients is subject to bias in the estimation of rain area fraction by the PR. This is a consequence of the limited PR swath size that does not always cover the entire precipitating system, and due to the limited number of precipitating systems used in the calibration period. To account for this effect, bias adjustment coefficients are determined in the calibration period for each T_{mode} category by evaluating the ratios of retrieved rain areas to the corresponding PR rain areas. The bias adjustment is applied on the A_{rain} estimates derived from Eqns. (1a) and (1b).

The next step consists of determining the convective rain area fraction, which is defined as a function of the area under T_{mode} (A_{Tmode}), cloud area (A_{cloud}), and the area of pixels with lightning ($A_{lightning}$) in the case of LTG clouds. The basis for using the last predictor is the hypothesis that lightning is a proxy for convective cores. Therefore, regions with lightning observations can be used to define the degree of active convection in a LTG cloud. Scatter plots (not shown here) of convective rain area ($A_{convective}$) versus A_{Tmode}/A_{cloud} and $A_{lightning}/A_{cloud}$ area ratios for NLTG and LTG clouds and for different T_{mode} categories were used to derive power law relationships, which are presented in Figures 3c,d. Accordingly, the fraction of convective rain area is related to A_{Tmode}/A_{cloud} (or $A_{lightning}/A_{cloud}$) ratios as follows:

$$A_{convective}(\%) = a(A_{Tmode}/A_{cloud})_{Tmode}^{b} \text{ , NLTG clouds} \quad (2a)$$

$$A_{convective}(\%) = a(A_{lightning}/A_{cloud})_{Tmode}^{b} \text{ , LTG clouds} \quad (2b)$$

It is noted from Figure 3c that the fraction of convective rain area shows distinction between land and ocean clouds for T_{mode} bins above 225 K and NLTG clouds, while for clouds with T_{mode} below 225 K the scatter plots suggested a single parameterization for both land and ocean clouds. This shows that ocean clouds are subject to larger convective fraction than land clouds for the same T_{mode} distributions. A more extensive analysis and longer calibration periods are necessary to obtain a more definitive evaluation of these intrinsic relationships.

Finally, having determined the convective rain area, the stratiform area is defined as the remaining rain area of the cloud system. The steps involved in the convective/stratiform rain area estimation are summarized as follows:

1. Delineate cloud clusters with temperature below 258 K in the IR array and evaluate their area (A_{cloud}).
2. Evaluate the T_{mode} value and A_{Tmode} for each cloud cluster.
3. Accumulate lightning observations for a time window ±7.5 minutes around the IR image time (the specific time is when GOES-8 scanner crosses the equator) and apply the detection efficiency of STARNET.
4. Classify clouds as LTG and NLTG clusters according to the lightning presence.
5. Compute the lightning area for the LTG clouds.
6. Evaluate rain area and convective area for each cluster according to LTG and NLTG cloud relationships as a function of T_{mode}.
7. Define the remaining area (A_{rain}-$A_{convective}$) as stratiform

8. Compute the IR Tb histogram below T_{mode} and enumerate the IR pixels from the lowest to the warmest temperatures.
9. Apply convective rain area:
   - For LTG Clouds: Assign convective class index to lightning pixels first, and subsequently to the pixels with lowest IR temperatures until reaching the fraction of convective rain area.
   - For NLTG Clouds: Assign convective class index to the lowest IR temperature pixels until reaching the fraction of convective rain area.
10. Apply stratiform rain class to the coldest pixels beginning at the end of the convective IR pixels until reaching the total rain area.

Characteristic examples of the proposed technique applied on STARNET and GOES IR data are illustrated in Figures 4 and 5, which show rain areas with convective and stratiform partitions as retrieved by SIRT and TRMM-PR. The top panels show GOES-IR images on a gray scale and matched STARNET lightning measurements in a 15-minute time window. The blue contour represents the 258 K isotherm. The middle and bottom panels show the SIRT and PR retrieved convective and stratiform rain areas, respectively. We show only rain areas above 0.5 mmh^{-1} to be consistent with the PR measurement sensitivity (18 dBZ) (Iguchi et al. 2000). Figures 6a through 6d show vertical cross-sections of TRMM-PR at selected storms in Figures 4 and 5 that are labeled (A1-A2). Additionally the mixed phase region is displayed in these figures. The 0^{o} and -20 ^{o}C isotherms define this region, where it is believed to be the negative charge center and the region for the most favorable charge separation (Williams, 1985).

Figure 4a presents an isolated cloud cluster over the Amazon region. Both SIRT and PR show almost the same area. In this case no lightning was detected by STARNET, but the Lightning Imaging Sensor (LIS) onboard TRMM (Christian et al., 1999) observed ten flashes at that cluster. Nevertheless, SIRT was able to define the convective region similar to PR. The vertical cross-section of this cluster presented in Figure 6a shows two convective cores that extended above 10 km. Higher reflectivity values (above 35 dBZ) are not predominant in the mixed phase region, which according to Toracinta et al (1996) would be characterized by strong negative cloud-to-ground lightning flashes. Therefore, this observation would suggest that weak strokes associated with intra-cloud lightning were predominant in the cloud system. Additionally, Morales et al. (2002b) have shown that in this region STARNET lightning measurements have low detection efficiency (~10%), also see Figure 1, and are associated with significant location error, both of which can compromise rain retrieval accuracy.

Figure 4b shows a squall line moving over Cuba. Lightning locations show good agreement with the convective regions observed by the PR. The cross-section in Figure 6b shows vigorous convective cores reaching 12 km. Reflectivity values between 35-50 dBZ are observed in the mixed phase region. This explains the high lightning rate observed along this squall line. In this example both rain area and its convective fraction estimated by SIRT exceed the corresponding PR estimates. This is probably due to the high lightning rate associated with a longer time interval, while PR only observed an instantaneous snapshot of the precipitation field.

Figure 5a shows a winter frontal system moving eastward off the coast of Florida. The lightning measurements offer a good delineation of the convective cores of this system, even though it showed a larger area than the PR. The cross-section in Figure 6c shows two convective towers that have a reflectivity factor above 35 dBZ in the mixed phase region. The first core

reaches 9 km height, which explains the presence of lightning. It is worth noting the technique's effectiveness in removing most of the cold cirrus contamination, shown by the large cloudiness in the figure. Comparisons with PR show moderate overestimation on the rain area, but also ability to detect some of the small convective features of the observed system.

Finally, Figure 5b presents a winter cloud system over the Gulf of Mexico. Note that the lightning measurements are over the convective region defined by the PR. The vertical cross-section in Figure 6d shows a deep convective core reaching 12 km height with high reflectivity factor below the freezing level. Note that along this vertical thunderstorm slice, regions of precipitation are associated with lightning observations. The rain area is moderately overestimated by SIRT, which again may have to do with the instantaneous PR measurement. In all four examples presented above SIRT showed an indication of removing the cirrus contamination and to represent the rain area phase, with the estimated convective area consistent with the PR measurements.

4. Assignment of rainfall rates

The expressions for computing rainfall rates are evaluated in a probabilistic way (Calheiros and Zawadski, 1987) that relates the same quantiles of precipitation parameters and IR brightness temperature and lightning rates. In this methodology, it is assumed that the lowest temperatures and highest rates of lightning would be correlated with the most intense precipitation. In regions of the probability matching that are susceptible to insufficient sampling (i.e., tails of the cumulative distributions) the relationships are determined through fitting of a continuous function.

The above probabilistic relationships have been compiled differently for NLTG and LTG clouds as well as land versus ocean backgrounds. Furthermore, different relationships have been computed for convective and stratiform rain parameters as a function of each T_{mode} class interval. The two months calibration period is not sufficient to further refine the relationships associated with the climatological differences between regions of the study domain. Consequently, calibration relationships are based on data from the entire study area, even though this approach introduces uncertainty associated with the natural variability of systems acting over meteorologically different regimes in the domain of study. The following steps are involved in assigning rainfall rates in the delineated convective and stratiform rain areas:

LTG clouds:

a) The convective area is divided in two parts:

- Lightning area (pixels having lightning);
- Remaining convective area, pixels without lightning;

b) Assigning convective and stratiform rainfall:

- Assign the rainfall rates in the lightning area as a function of the lightning rate;
- Assign the rainfall rates in the non-lightning convective rain area using the IR brightness temperature-rainfall relationships;
- Apply the correspondent stratiform rainfall relationships to the IR brightness temperatures in the stratiform area.

NLTG clouds:

a) Assigning convective rainfall: Apply the convective rainfall relationships to the IR brightness temperatures in the convective area;

b) Assigning stratiform rainfall: Apply the correspondent stratiform rainfall relationships to the IR brightness temperatures in the stratiform area.

5. Algorithm Evaluation

5.1 Comparison with TRMM-PR

A total of 326 independent TRMM overpasses from February 1998 have been used in the analysis. In this period, we identified a significant number of raining cloud systems with area coverage greater than 100x100 km: namely, 203 LTG and 1,499 NLTG clouds. The current analysis concentrates on evaluating the algorithm error statistics in determining the rain areas and volumes (i.e., sum of rain rates within a rain area) of the cloud systems, as well as the instantaneous rainfall rate at varying spatial resolutions. The evaluation is performed separately for LTG and NLTG clouds, convective and stratiform rain types. The cloud type separation illustrates that LTG clouds are responsible for the most intense precipitation and in the absence of lightning information this rainfall distribution is likely to be incorrectly depicted by IR.

The analysis uses the correlation coefficient (CC), fraction standard error (FSE), and normalized bias (NBIAS) as the statistical measures of SIRT retrieval error. These coefficients are defined as follows:

$$CC = \frac{\frac{1}{N}\sum_{i=1}^{N} R_i^T R_i^S - \frac{1}{N^2}\sum_{i=1}^{N} R_i^T \sum_{i=1}^{N} R_i^S}{\frac{1}{N}\sqrt{\sum_{i=1}^{N}\left(R_i^T - R_{mean}^T\right)^2 \sum_{i=1}^{N}\left(R_i^S - R_{mean}^S\right)^2}} \qquad (3)$$

$$FSE(\%) = 100 \sqrt{\frac{\frac{1}{N}\sum_{i=1}^{N}\left(R_i^T - R_i^S\right)^2}{\frac{1}{N}\sum_{i=1}^{N}\left(R_i^T - R_{mean}^T\right)^2}} \tag{4}$$

$$NBIAS(\%) = 100 \frac{\frac{1}{N}\sum_{i=1}^{N}\left(R_i^S - R_i^T\right)}{\frac{1}{N}\sum_{i=1}^{N} R_i^T} \tag{5}$$

where N is the total number of clouds, while R^T and R^S are the reference ("true", TRMM-PR or rain gauges) and SIRT estimated variables, respectively. For example, in evaluating the technique's rain volume estimates, N would be the number of matched clouds falling in a selected category, while R^T and R^S would be the rain volume (m^3) from PR and SIRT, respectively. The CC varies from 0 to 1 representing a range of none to high correlation between the two variables. The FSE can be thought of as the error variance normalized by the variance of the predicted variable. The smaller the value, the less the variability of the error is with respect to the natural variability of rainfall. The NBIAS represents the fraction of overestimation (>0) or underestimation (<0) with respect to the reference value.

a) Rain Area and Rain Volume

Figure 7 shows scatter plots of PR versus SIRT rain areas for both cloud types, while Tables 1 and 2 show the respective difference ("error") statistics. The left panels of Figure 7 correspond to the total rain areas, center panels to convective areas, and right panels to stratiform areas. It is noted that the rain areas defined by LTG clouds exhibit smaller error variability than NLTG clouds. LTG clouds are associated with larger convective areas than NLTG clouds. In both cloud types SIRT underestimates the rain area. The underestimation bias (NBIAS) is 21.5% for LTG clouds and 29.1% for NLTG clouds, showing a somewhat better performance in

determining LTG cloud rain areas. The convective area is also underestimated in both cloud types, but in LTG clouds SIRT tends to perform better when systems are large. In the stratiform regions, there is a tendency to underestimate rain area for larger cloud systems (i.e., above 10 degree^2). The biases are lower for LTG (-21.83%) clouds compared to the NLTG (-29.15%) clouds. The correlation in both cloud types is high, while FSE for LTG clouds is about 36%. These results show higher correlation and less error variability in the LTG cloud estimates, especially the ones related to the convective rain areas. This clearly indicates that lightning information can contribute significantly to the improvement of rain area determination as well as the proper delineation to its convective and stratiform regions.

Figure 8 shows the corresponding rain volume scatter plots of total, convective, and stratiform rain volumes for both LTG and NLTG clouds. Note the lower variability exhibited in the LTG clouds compared to NLTG clouds. The rain volume overestimation bias for NLTG and LTG clouds is 12.5% and 19.5%, respectively. The larger NBIAS and FSE retrieved in LTG compared to NLTG clouds can be due to their higher (one order of magnitude) rain rate magnitudes and variability associated with active systems, which tends to intensify rain errors. Furthermore, the small number of LTG cloud systems included in the statistics also contributes to biasing in the error statistics evaluation, an effect of which can be the higher correlation shown for NLTG clouds in convective rain type**.** As shown in Tables 1 and 2 SIRT overestimates and underestimates, respectively, convective and stratiform rain volumes. The separation by rain type illustrates that the convective rain areas are responsible for most of the rain volume overestimation.

b) Instantaneous Rainfall Rate

Representative examples of the proposed technique's performance in retrieving instantaneous surface rainfall rate are presented in Figures 9 and 10 for the same examples presented in Figures 4 and 5. These plots show only surface rainfall rates above 0.5 mmh^{-1} since the minimum detectable reflectivity factor of PR is approximately 18 dBZ. The top and bottom panels show the surface rainfall rates retrieved by SIRT and PR, respectively.

In Figure 9a, PR measures a localized convective core, which is overestimated by SIRT. Despite this fact, SIRT is consistent with the PR measurements in assigning higher rainfall rates in the core of convection and low intensity rain elsewhere. Overall, in this instantaneous case SIRT overestimates rain area by 6% and rain volume by about 300%.

The SIRT rainfall estimates in Figure 9b show good agreement with the PR measurements, particularly in defining the high rain intensities over the convective cores, which were associated with the presence of lightning. Additionally, SIRT was able to define properly the regions of low intensity and filter some of the non-rainy cloudiness associated with cirrus contamination. Overall, in this example SIRT overestimated rain area by 20% and the rain volume by 19% (see Figure 4b).

For the storm case of Figure 10a, where Figure 5a shows to be associated with a large cloud shield, the lightning information seems to help with the delineation of the convective cores. The rain estimates of SIRT are comparable to the ones observed by the PR, where SIRT overestimates the rain area by 25% and rain volume by 36%. Finally, in the case of Figure 10b the SIRT rain estimates are also comparable to the PR measurements, even though the rain area is overestimated. The lightning information helped with the identification of the convective

cores as shown by comparisons with the PR classification. The overall bias for SIRT rain estimate in this case is an overestimation of the rain area by 100% and 133% for the rain volume.

c) Rainfall Rate Distribution

This section presents a comparison of the convective and stratiform rainfall distributions between SIRT and PR estimates. Figures 11 and 12 show these comparisons for LTG and NLTG clouds. The LTG clouds, Figure 11, have a convective rainfall rate mode at around 12 mmh^{-1} according to the technique estimates, while the PR has a more flat distribution with mode at around 20 mmh^{-1}. The LTG cloud stratiform rainfall rate distribution derived by SIRT is quite similar to the PR estimates. PR and SIRT convective rain rate estimates for NLTG clouds have comparable distributions as shown in Figure 12 and the mode of their distributions is around 6-7 mmh^{-1} for both estimates. In stratiform rain, SIRT estimates histogram resembles greatly the PR histogram. The NLTG stratiform rain histograms tail off at approximately 5 mmh^{-1}, while in the LTG clouds the intensities tail off close to 7 mmh^{-1}. It is evident comparing the presented frequency plots that LTG clouds reach higher rainfall intensities than NLTG clouds. Overall, the results show that the technique tends to underestimate (overestimate) low (high) intensity rain rates in convective systems for LTG clouds, while this effect is less apparent in NLTG clouds. It is noted that the small number of convective pixels in the LTG cloud sample (203 clouds) is not adequate to reproduce the actual rainfall distribution for those systems, which may partially explain the convective rainfall distribution differences observed in those clouds. Another explanation is potential deficiencies of SIRT algorithm in assigning the proper convective rainfall rates in areas with heavy precipitation where saturation of IR and lightning signals occur.

5.2 Comparison with rain gauges

In this section, SIRT estimates are compared against independent measurements from a rain gauge network in Florida, United States. The spatial distribution of the rain gauge network is presented in Figure 13. The rain gauge network consisted of 150 tipping buckets with temporal resolution ranging from 1 to 5 minute intervals and has been quality controlled by the TRMM office of NASA Goddard Space Flight Center (personal communication of Mr. Brad Fisher). Rain gauge measurements and SIRT estimates are averaged over coincident grids of varying spatial resolutions, i.e., 0.1x0.1, 0.2x0.2, 0.5x0.5, 1x1, and 2x2 degree boxes, and aggregated to hourly and monthly accumulations. Attention is paid to minimize the gaps in the validation gauge data by excluding from the analysis rain gauge locations with reports during less than 70% of the three-month period. Rain gauges measure rainfall at a very small spatial scale, therefore, the representativeness of those measurements to the mean rainfall of areas with 8-10 orders of magnitude larger scales is expected to be affected by the natural variability of precipitation processes (Kitchen and Blackall, 1992). Subsequently, any statistical comparison between area rainfall estimates of the technique and a limited number of gauge measurements should consider this effect in deriving the technique's error statistics (Anagnostou et al., 1999b). The selected grids and maximum and minimum number of gauges associated with each grid are listed in Table 3. The analysis concentrates on comparing histograms of coincident SIRT and PR hourly accumulations and evaluating the corresponding difference statistics (Eqns. 3-5).

Figure 14 shows the SIRT (broken line) and rain gauge (solid line) hourly rainfall histograms for various spatial scales. Overall, but more pronounced in the finer scales (e.g., 0.1 degrees), SIRT shows higher frequency at the low intensity rainfall rates, while rain gauges have higher frequency at the more intense precipitation. This is an expected outcome considering that

we compare point measurements to area average estimates. With decreasing the grid resolution, SIRT resembles more the rainfall rate distribution measured by rain gauges. It seems that 0.5 degrees resolution is the limit for this transition. Table 4 presents the error statistics of hourly rainfall rates for each grid resolution between SIRT and rain gauges. Overall, SIRT tends to overestimate the corresponding gauge rainfall. At 0.1 degrees resolution the mean bias NBIAS and FSE error statistics are 5.77% and 133%, respectively. It is noted that a significant portion of the FSE value is attributed to the natural variability of rainfall that affects the gauge area rainfall sampling**.** Past studies in the Florida region have shown that the gauge sampling error can attribute up to 50% of the observed sensor-gauge difference variance for hourly accumulation at similar spatial scales (Anagnostou et al. 1999b). The bias increases to 35% at 2 degree resolution, which may be due to the increased uncertainty in matching area and point rainfall estimates at that scale. The SIRT-gauge correlation is low (0.63), but this could be due to random effects associated with the huge sensor sampling differences. At monthly accumulations the bias of SIRT estimates is 2.4% and 0.27% for the 1x1 and 2x2 degree spatial scales, respectively.

6. Significance of lightning information

This section tests the significance of lightning information in surface rainfall estimation through comparisons with TRMM-PR and the Florida gauge network data. The no-lightning SIRT scheme is determined such that all cloud systems are now considered as NLTG. This approach compares two schemes (the current and one omitting lightning information) based on the same data resolution and calibration/validation periods.

First, we compare the two schemes in terms of their performance in determining the rain area and volume for the various storm systems observed by SIRT and TRMM-PR in the validation period of February 1998. Table 5 contains statistics of their errors. These error statistics indicate that lightning information improves rainfall estimation accuracy. In terms of rain area we find an overall bias reduction of 31%, and a decrease of FSE by 22%, which indicates decrease in error variance. In the rain volume comparison, the algorithm with lightning information has an overall bias of about 16% (overestimation) while without such information the bias is 24% (underestimation). This indicates that clouds with lightning have higher rain volumes as already stated in the methodology section and omitting this information can result to significant underestimation of the volume of rainfall. The FSE error increases for lightning information by about 20%, which we believe is an issue mostly associated with the algorithm parameter's regional variability and pure lightning location accuracy originating from the Amazon and Caribbean areas.

Finally we test the impact of lightning information by comparing non-lightning SIRT scheme estimates against the Florida rain gauge network measurements where STARNET lightning estimates have the highest accuracy. The methodology used to compare these estimates with the rain gauge accumulations is the same as presented in the previous section. Table 6 summarizes the non-lightning SIRT configuration error statistics as well as the bias reduction from non-lightning to lightning SIRT scenario for various spatial resolutions. It is shown that without lightning information the precipitation is underestimated at all spatial scales evaluated in this study. Overall, the comparison between lightning and non-lightning SIRT configurations reveals that there is a considerable increase of the relative fractional bias (NBIAS) and a decrease in the correlation coefficient (CC) when information is omitted (see Tables 4 and

6). This effect indicates that lightning observation can improve the identification of the deep convection, which is responsible for the higher rainfall amounts, and consequently, better separate those intense regions from the more stratiform low precipitation rate areas. It is also shown that the higher the resolution the better improvement is achievable by use of lightning.

At 0.1x0.1 degree non-lightning SIRT underestimated precipitation by ~46%; this bias is reduced by ~87% when accounting for lightning information. Similar numbers may be derived for the other spatial scales. At 0.2x0.2, 0.5x0.5, and 1x1 degree grid resolution the reduction of underestimation due to lightning information is 78%, 76% and 38%, respectively. The increase in correlation from SIRT without lightning to SIRT with lightning is 0.13, 0.06, 0.04, 0.04 and 0.03 for the range of 0.1 to 1 degree scales of aggregation. These results indicate that lightning measurements can indeed improve rainfall estimation by better identifying the convective and stratiform portions of a raining system at finer scales.

7. Conclusions

A technique that retrieves surface rainfall rates from a combination of observations from an experimental long-range lightning network and geo-stationary satellite infrared observations is described. This technique combined with coincident TRMM PR rainfall products presents a first effort towards advancing our current capabilities for continuous precipitation monitoring over large regions and high spatio-temporal resolutions with the use of lightning information. The hypothesis made in formulating the methodology is that lightning measurements can be associated with ice aloft; a better identification of rain and convective area is achieved by combining lightning and IR brightness temperature; and finally that the separation of

precipitating systems into clouds with lightning and without lightning can contribute to improving precipitation estimation.

Parameterizations for rain area estimation as well as the convective rain area delineation were developed for both lightning and lightning free precipitating clouds. These relationships are functions of cloud area defined by the 258 K isotherm, the area contained within the most frequent IR temperature (T_{mode}) in the cloud system, and the lightning area in the case of active clouds. The rainfall rate relationships were developed in a probabilistic way by matching the cumulative distributions of IR temperatures and lightning rates with the PR precipitation estimates. These functions were evaluated separately for convective and stratiform rain types, lightning and lightning free clouds, and for land versus ocean surfaces.

Two months (December 1997 and January 1998) of coincident data over a large region (i.e., 125W-45W in longitude and 40N-10S in latitude) were used for evaluating the algorithm parameters. The evaluation of this new technique was based on independent TRMM-PR orbits from the subsequent month (February 1998) and three months (December 1997 to February 1998) of rain gauge observations from a network in Florida.

The estimated rain areas are shown to be well determined when compared against rain areas observed by the PR. Overall, the technique underestimates both LTG (21.55%) and NLTG (29.14%) cloud rain areas. The error variability and correlation coefficients are 36.34% with respect to the rain area variance and 0.97 for LTG clouds, and 42.85% and 0.96 for NLTG clouds, which is quite satisfactory performance for an algorithm operating over a wide region extending from North to South America and portions of the Atlantic and Pacific oceans (~4,000 square degrees). LTG clouds show lower errors on the definition of convective and stratiform rain areas compared to the NLTG clouds, which is a physical consequence of the strong

association of lightning to convective rainfall. Moderate (~12%) positive bias is shown in rain volume estimates. These results indicate that SIRT assigns higher rainfall rates than PR measurements, which is likely a consequence of the rain area underestimation. The histograms of retrieved stratiform rainfall rates for both NLTG and LTG clouds are similar to those derived from PR in the validation period. The largest differences are apparent in the convective parts of LTG clouds where the low data sampling can be an issue.

Comparisons with validation rain gauge data revealed that the SIRT is able to represent the observed precipitation distribution at scales ranging from 100 km^2 to 4 $degree^2$ with low overall bias (5.7%).

Finally we investigated the significance of lightning information on rainfall estimation accuracy. In that respect, SIRT was set to run without lightning information, namely all clouds were set as NLTG. Comparisons with TRMM-PR showed that lightning information improves rainfall estimation accuracy when compared to the non-lightning scenario. In rain area determination there was an overall bias reduction of 31%. In rain volume the lightning information showed an overestimation of 16%, while the non-lightning scenario gave an underestimation of 24%. In rain gauge comparisons, the bias reduction from incorporating lightning data was more pronounced. It was up to 87% for 0.1 degrees estimates, while it dropped to about 38% and 9% for the 1 and 2-degree estimates. The increase in correlation was up to 0.05 and 0.13 for instantaneous PR and hourly gauge validation data, accordingly.

The experimental long-range lightning network used in this study is no longer operational. A new network of the same type was deployed in Europe this summer by the National Observatory of Athens. The network consist of six stations located in Larnaca

(Cyprus), Mt. Etna (Italy), Evora (Portugal), Birmingham (UK), and Iasi (Romania), and will set the ground for further development in the direction of continuous thunderstorm monitoring.

Acknowledgements: We acknowledge and appreciate useful discussions and input from Dr. James Weinman of NASA/GSFC, Dr. Steve Goodman of NASA/MSFC, and Dr. Earle Williams of MIT. This study was supported by NASA New Investigator Program award under Grant NAG5-8636. This research uses the Sferics Timing and Ranging Network (STARNET) project funded by NASA Small Business Innovative Research grant NAS5-32825. TRMM-PR and rain gauges data were available by the TRMM Science Data and Information System (TSDIS) of NASA/GSFC and the Distributed Active Archive Center (DAAC) of NASA/GSFC. TRMM-LIS data were provided by Global Hydrologic Resource Center of NASA/MSFC and the Space Science Engineering Center (SSEC) of University of Wisconsin provided the GOES-8 imagery.

8. References

Adler, R.F. and A.J.Negri, 1988: A satellite infrared technique to estimate tropical convective and stratiform rainfall. J. Appl. Meteor., 27, pp. 30-51.

Anagnostou, E.N., A.J. Negri, and R.F. Adler, 1999a: A satellite infrared technique for diurnal rainfall variability studies, *J. of Geoph. Res.-Atmos.*, 104 (D24), 31,477-488.

Anagnostou, E.N., W.F. Krajewski, and J. Smith, 1999b: Uncertainty quantification of mean-field radar-rainfall estimates, J. Atmos. Ocean. Techn., 16, pp. 206-215.

Arkin, P.A., 1979: The relationship between fractional coverage of high cloud and rainfall accumulations during GATE over the B-scale array. Mon. Wea. Rev., 107,1382-1387.

Arkin, P.A., and B. N. Meisner, 1987: The relationship between large-scale convective rainfall and cold cloud over the Western Hemisphere during 1982-1984. Mon. Wea. Rev., 115, pp. 51-74.

Awaka, J., T. Iguchi, H. Kumagai, and K. Okamoto, 1997: Rain type classification algorithm for TRMM precipitation radar. Proceedings of the IEEE 1997 Int. Geosc. R. Sens. Symp., August 3-8, Singapore, pp. 1636-1638.

Baker, M.B., H.J. Christian, J. Latham, 1995: A computational study of the relationships linking lightning frequency and other thundercloud parameters, Q. J. R. Meteorol. Soc., 121, pp. 1525-1548.

Buechler, D., H.J. Chirstian, S.J. Goodman, 1994: Rainfall estimation using lightning data. Seventh Conf. Satell. Meteor. and Ocean., Amer. Meteorol. Soc., June 6-10, pp. 171-174.

Calheiros, R. V., and I. Zawadzki, 1987: Reflectivity rain-rate relationships for radar hydrology in Brazil. J. Climate Appl. Meteor., 26, 118–132.

Christian, H.J., R.J. Blakeslee, S.J. Goodman, D.A. Mach, M.F. Stewart, D.E. Buechler, W.J. Koshak, J.M. Hall, W.L. Boeck, K.T. Driscoll, and D.J. Boccippio, 1999: The Lightning Imaging Sensor. Proceedings of the 11th Int. Conf. on Atmos. Electricity, Guntersville, Alabama, 746-749.

Cramer, J.A. and K.K. Cummins, 1999: Long-Range and Trans-Oceanic Lightning detection, 11th International Conf. Atmos. Electricity, 376-379.

Goodman , S.J., 1990: Predicting thunderstorms evolution using ground-based lightning detection networks. NASA Tech. Memo. TM-103521.

Grecu, M., E.N. Anagnostou, R.F. Adler, 2000: Assessment of the use of lightning information in satellite infrared rainfall estimation. J. Hydrometeor., vol. 1, 3, pp. 211-221.

Iguchi T, R. Meneghini, J. Awaka, T. Kozu, K. Okamoto, 2000: Rain profiling algorithm for TRMM precipitation radar data. Remote Sensing and Appl. Earth, Atmos. Oceans, vol. 25, 5, pp. 973-976.

Kitchen, M., and R.M. Blackall, 1992: Representativeness errors in comparisons between radar and gauge measurements of rainfall. J. Hydrol., 134, pp. 13-33.

Kummerow, C., W. Barnes, T. Kozu, J. Shiu and J. Simpson, 1998: The tropical rainfall measuring mission (TRMM) sensor package, J. Atmos. And Oceanic Tech., 15, 3, 809-817.

Lee, A.C.L., 1986: An operational system for the remote location of lightning flashes using a VLF arrival time difference technique, J. Atmos. and Ocean. Tech., 3, pp. 630-642.

Morales, C.A., J.A. Weinman, J.S. Kriz, and G.D. Alexander, 1997: Thunderstorm distributions from NASA/RDI sferics observing system. AGU, Fall, San Francisco, US.

Morales, C.A., E.N. Anagnostou, J.A., Weinman, and S. Kriz, 2002a: Continuous Long-Range Thunderstorm Monitoring by a VLF Receiver Network. Part I: Location Error Analysis, *J. Atmos. and Ocean. Techn*. (submitted).

Morales, C.A., E.N. Anagnostou, and J.A., Weinman, 2002b: Continuous Long-Range Thunderstorm Monitoring by a VLF Receiver Network. Part II: Detection Efficiency, *J. Atmos. and Ocean. Techn*. (submitted).

Petersen, W.A. and S.A. Rutledge, 1996: Characteristic differences in cloud-to-ground lightning flash densities and rain yields for different climate regions. Int. Conf. On Atmos. Elec., June 10-14, Osaka, Japan.

Petersen, W.A. and S.A. Rutledge, 1998: On the relationships between cloud-to-ground lightning and convective rainfall, J. Geophys. Res. Atmos., 103,D12, 14025-14040.

Simpson, J., C. Kummerow, W.K. Tao, and R.F. Adler, 1996: On the tropical rainfall measuring mission (TRMM). Meteorol. Atmos. Phys., vol 60, pp.19-36.

Tappia, A., J.A. Smith, and M. Dixon, 1998: Estimation of convective rainfall from lightning observations, J. Appl. Meteor., 37, 1497-1509.

Toracinta, E.R., K.I. Mohr, E.J. Zipser, R.E. Orville, 1996: A comparison of WSR-88D reflectivities, SSM/I brightness temperatures, and lightning for mesoscale convective systems in Texas. Part I: radar reflectivity and lightning. J. Appl. Met., 35, pp. 902-918.

Vicente G.A., R.A. Scofield, W.P. Menzel, 1998: The operational GOES infrared rainfall estimation technique. Bull. Amer. Meteorol. Soc., vol. 79, 9, pp. 1883-1898.

Williams, E.R., 1985: Large-scale charge separation in thunderclouds, J. Geophys. Res., 90, 6013-6025.

Workman, E.J. and S.E. Reynold, 1949: Electrical activity related to thunderstorm growth. Bull. Amer. Meteor. Soc., 30, pp. 142-145.

	Rain Volume (m^3)			Rain Area ($degree^2$)		
LTG	**CC**	**FSE(%)**	**NBIAS(%)**	**CC**	**FSE(%)**	**NBIAS(%)**
Convective	0.64	220.12	46.79	0.87	76.79	-20.52
Stratiform	0.77	84.92	-45.57	0.97	37.18	-21.83
Total	0.67	164.52	19.54	0.97	36.34	-21.55

Table 1. Correlation Coefficient (CC), Fractional Standard Error (FSE) and Normalized Bias (NBIAS) error statistics for SIRT rain volume and rain area for LTG clouds.

	Rain Volume (m^3)			Rain Area ($degree^2$)		
NLTG	**CC**	**FSE(%)**	**NBIAS(%)**	**CC**	**FSE(%)**	**NBIAS(%)**
Convective	0.76	128.31	52.61	0.72	104.09	-29.11
Stratiform	0.82	73.74	-31.94	0.96	43.61	-29.15
Total	0.82	94.26	12.52	0.96	42.85	-29.14

Table 2. Correlation Coefficient (CC), Fractional Standard Error (FSE) and Normalized Bias (NBIAS) error statistics for SIRT rain volume and rain area for NLTG clouds.

Resolution (degree^2)	Number of grids	Maximum number of gauges	Minimum number of gauges
0.1 x 0.1	4	12	03
0.2 x 0.2	6	15	04
0.5 x 0.5	4	42	10
1.0 x 1.0	4	75	11
2.0 x 2.0	3	82	15

Table 3. Grids selected in the SIRT-gauge intercomparison. From left to right the columns show the grid resolution and number, and maximum and minimum available number of gauges at all times.

Resolution (degree^2)	CC	FSE(%)	NBIAS(%)
0.1 x 0.1	0.62	133.5	5.77
0.2 x 0.2	0.61	135.5	9.48
0.5 x 0.5	0.63	149.2	9.64
1.0 x 1.0	0.64	159.0	23.58
2.0 x 2.0	0.61	153.7	35.43

Table 4: Correlation Coefficient (CC), Fractional Standard Error (FSE) and Normalized Bias (NBIAS) statistics SIRT-gauge rainfall differences evaluated for the different grid resolutions.

Rain Area Estimate	CC	FSE(%)	NBIAS(%)
With	0.97	37.43	-26.08
Without	0.95	48.23	-37.83
Rain Volume Estimate	CC	FSE(%)	NBIAS(%)
With	0.75	133.98	16.66
Without	0.70	107.44	-24.07

Table 5. Error statistics of rain area and rain volume for both SIRT schemes: with and without lightning information. Error was evaluated based on all storms measured by PR and SIRT.

Resolution (degree^2)	CC	FSE(%)	NBIAS(%)	Bias Reduction(%)
0.1 x 0.1	0.49	109.56	-46.52	87.59
0.2 x 0.2	0.55	108.53	-43.20	78.05
0.5 x 0.5	0.59	114.36	-41.46	76.74
1.0 x 1.0	0.60	115.71	-37.63	38.33
2.0 x 2.0	0.58	108.46	-39.10	9.38
Monthly Estimates				
1.0 x 1.0	----	--------	-53.00	95.47
2.0 x 2.0	----	--------	-55.00	99.50

Table 6. Correlation Coefficient (CC), Fractional Standard Error (FSE) and Normalized Bias (NBIAS) statistics for non-lighting SIRT-gauge rainfall differences evaluated for the different grid resolutions. Last column shows the relative bias reduction with respect to the non-lightning scenario.

List of Figures

Figure 11: Stratiform (left panel) and convective (right panel) rainfall rate histograms for TRMM-PR (red line) and SIRT (blue line) for LTG clouds during February 1998.

Figure 12: Same as in Figure 11 but for NLTG clouds during February 1998.

Figure 13: Configuration of the rain gauge network used in the study.

Figure 14: Hourly rainfall distributions derived from rain gauges (dark strips) and SIRT (white strips) for 0.1x0.1, 0.2x0.2, 0.5x0.5, 1x1, and 2x2 degree resolution. Solid dark gray bar represents common rainfall frequency observed by gauges and SIRT.

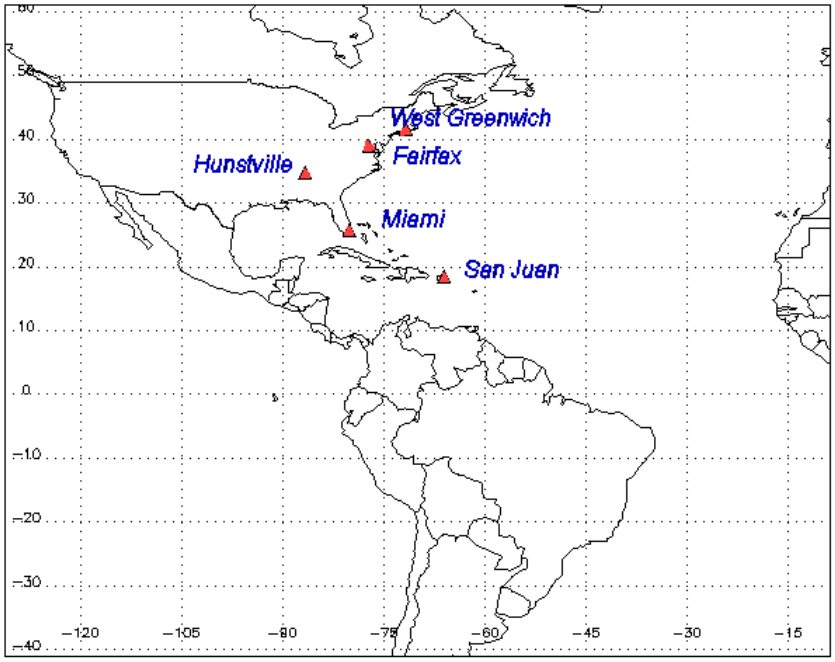

Figure 1. Location of STARNET radio receivers.

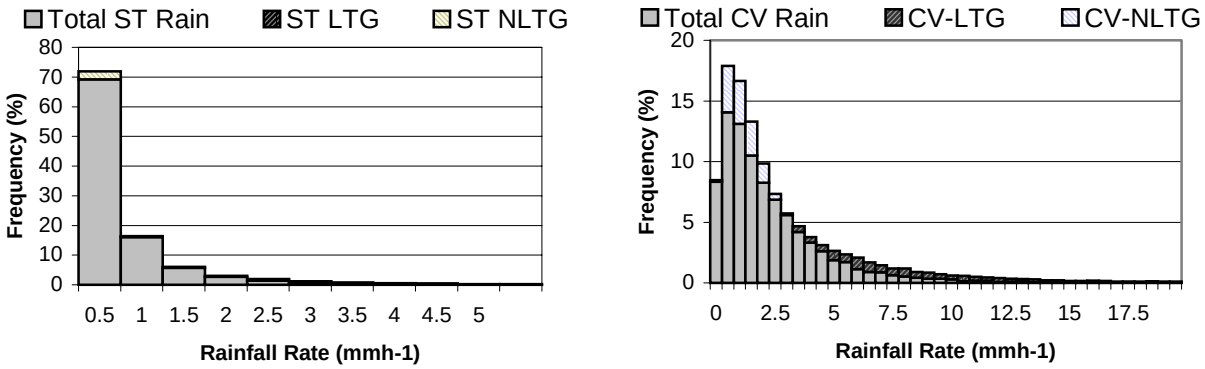

Figure 2: PR rainfall distribution for convective (right) and stratiform (left) rain types and LTG (solid stripes) versus NLTG (gray stripes) cloud cases. Solid gray bar represent common rainfall rate observed by for classification types.

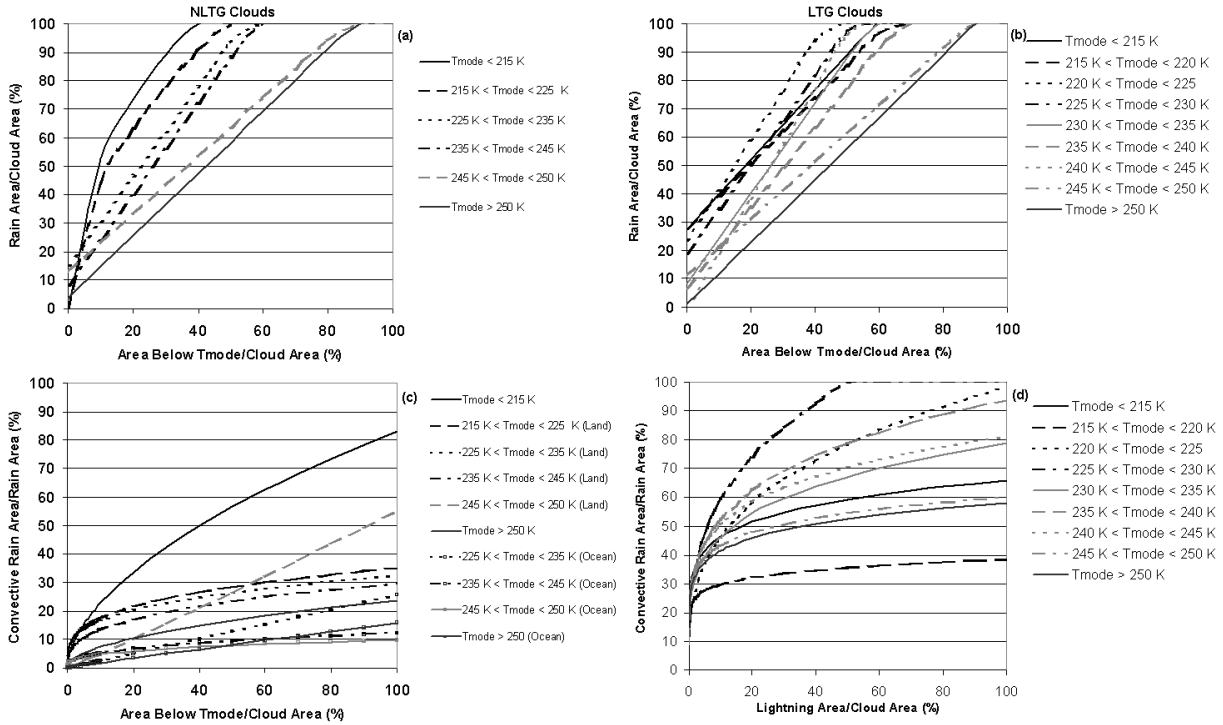

Figure 3: Least Square fit of (a) rain to cloud area fraction versus T_{mode} to cloud area fraction for NLTG and (b) LTG; and least square fit of (c) convective rain area fraction versus T_{mode} to cloud area ratios for NLTG, and (d) convective rain area fraction versus lightning to cloud area ratios for LTG clouds.

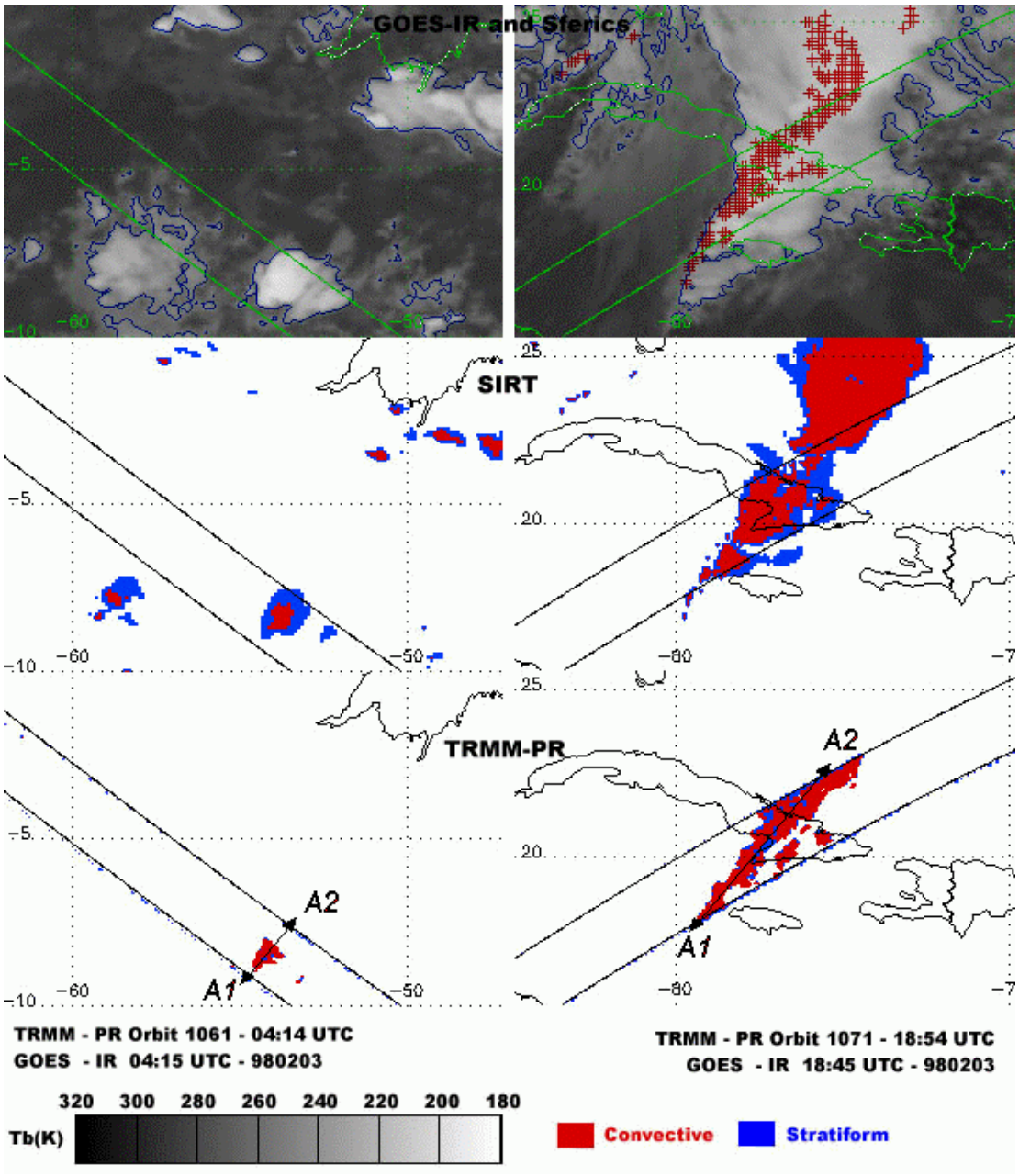

Figure 4: Top panel: GOES IR (gray scale) and lightning (red cross symbol) measurements. Middle and bottom panels show rain area retrieved by SIRT and coincident TRMM-PR overpass with the convective (red) and stratiform (blue) delineation. (a) Left column, February 3rd 1998 at 04:15 UTC and TRMM orbit 1061; (b) Right column, February 3rd 1998 at 18:45 UTC and TRMM orbit 1071

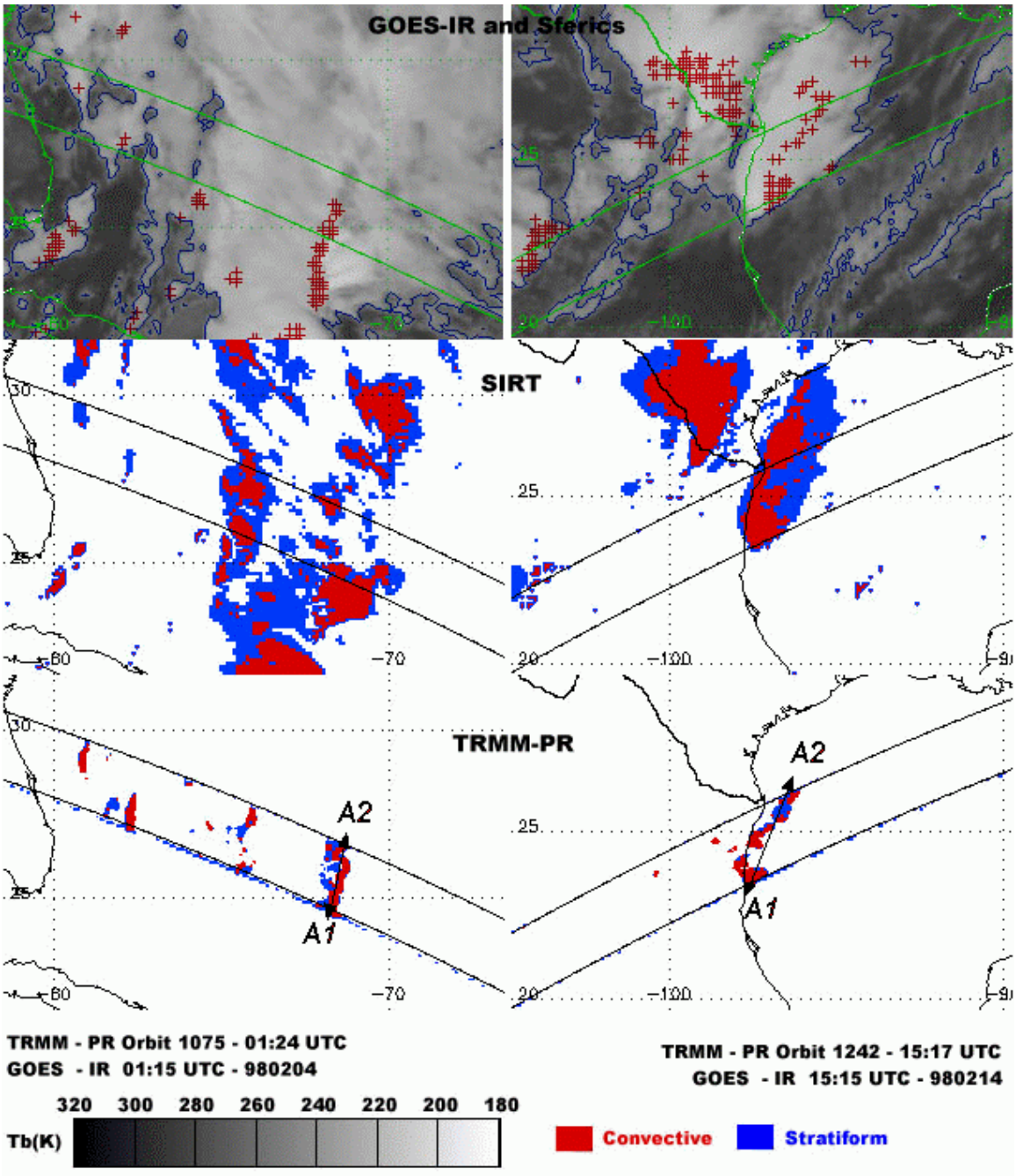

Figure 5. The same as in Figure 4 but (a) left column is for February 4th 1998 at 01:15 UTC and TRMM orbit 1075; and (b) right column for February 14th 1998 at 15:15 UTC and TRMM orbit 1242.

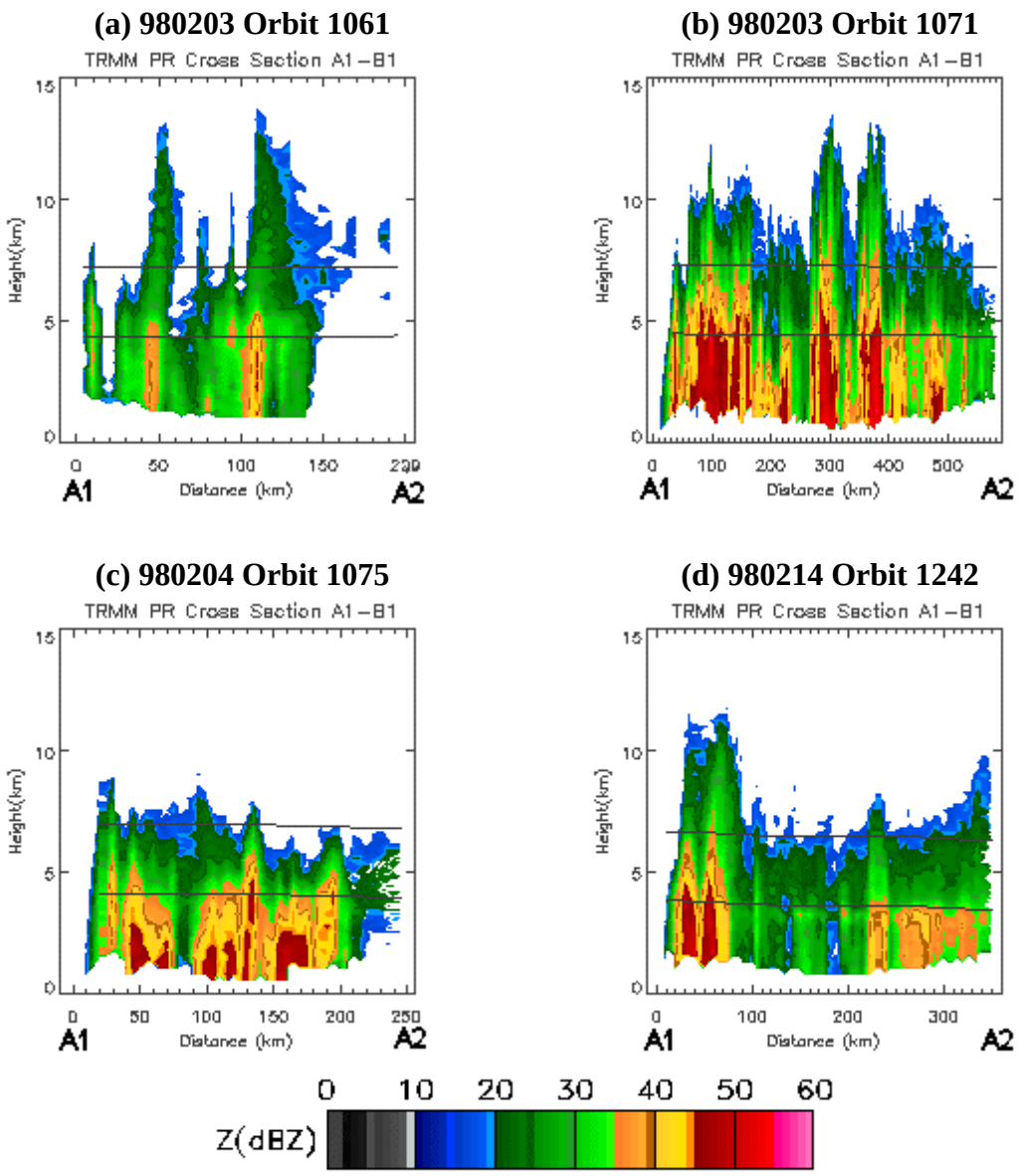

Figure 6. Vertical cross-sections at selected locations in the storm cases presented in Figures 4 and 5 as observed by TRMM-PR. The horizontal lines represent the mixed phase region bounded by the freezing level (0 ^{o}C isotherm) as determined by PR and the -20 ^{o}C isotherm assuming a pseudo-adiabatic temperature profile. (a) top left panel, cross-section for Figure 4a; (b) top right panel, cross-section for Figure 5b; (c) bottom left panel, cross-section for Figure 5a and; (d) bottom right panel, cross-section for Figure 5b.

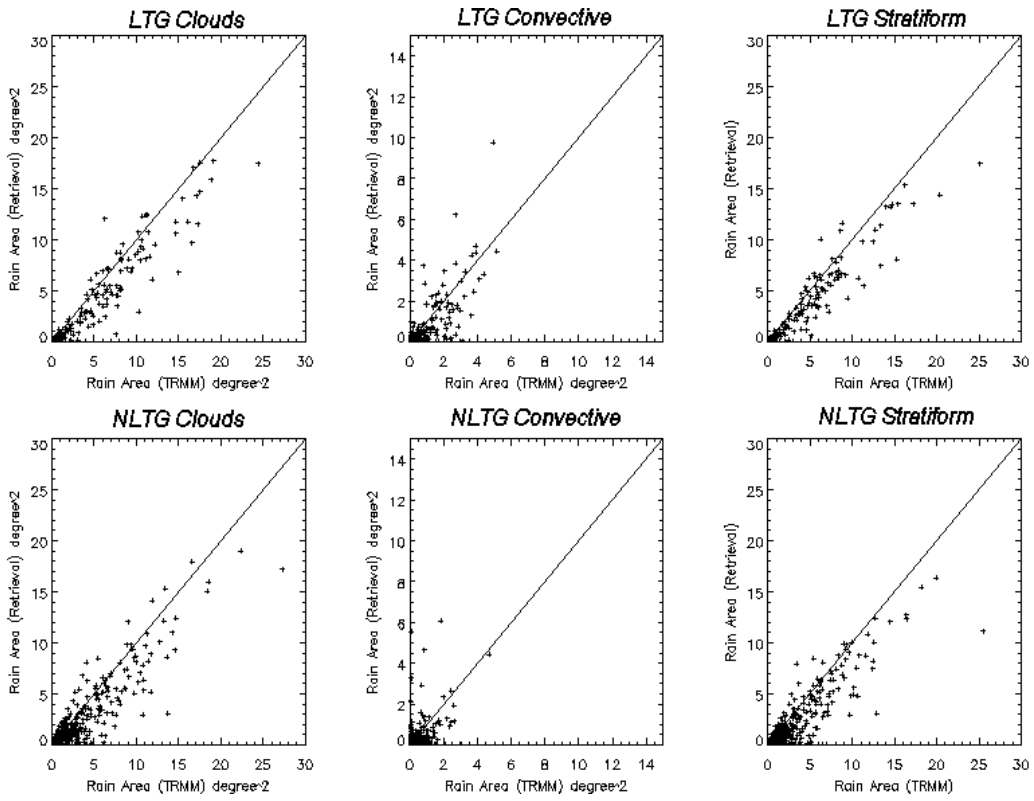

Figure 7: Scatter plots of rain area (in square degrees) retrieved by TRMM-PR versus SIRT. The top panels are for LTG clouds and the bottom represent the NLTG clouds. Total rain area is shown on the left panels, while the center and right panels show convective and stratiform rain areas, respectively.

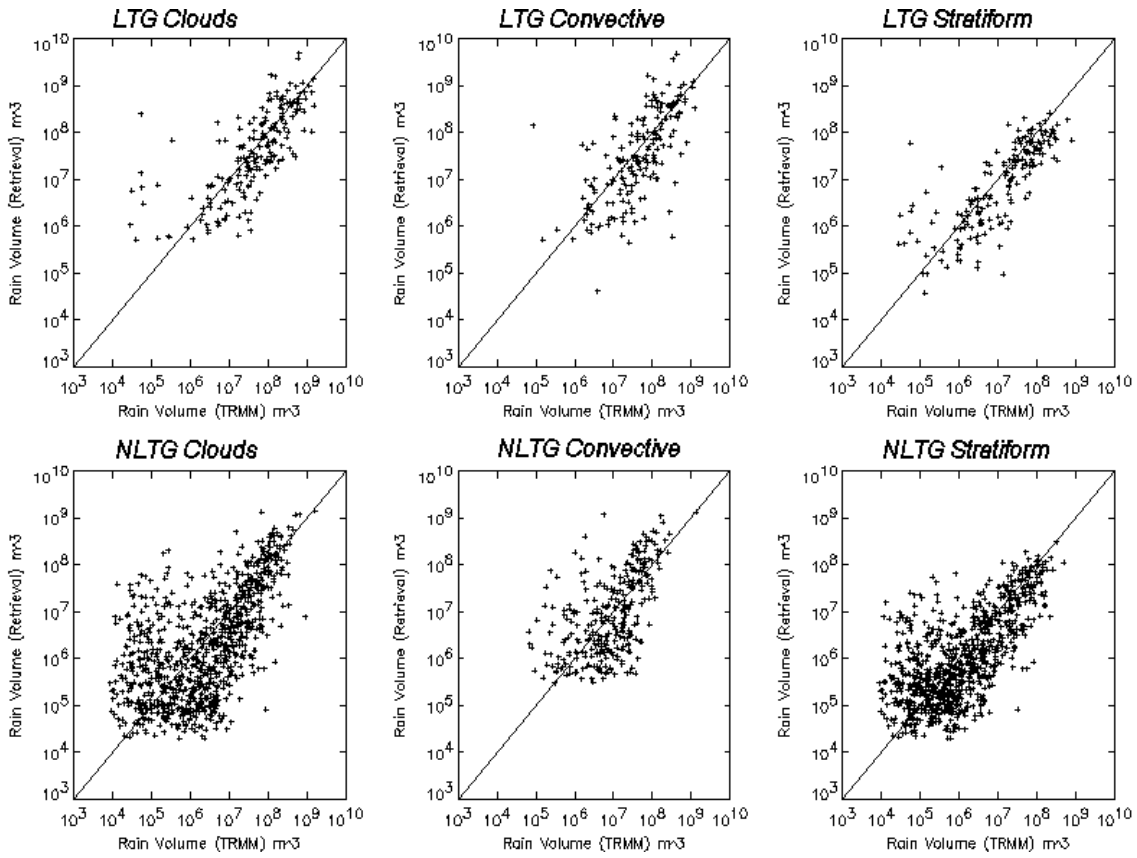

Figure 8: The same as in Figure 7 but scatter plots are for rain volumes (in cubic meter) retrieved by TRMM-PR versus SIRT.

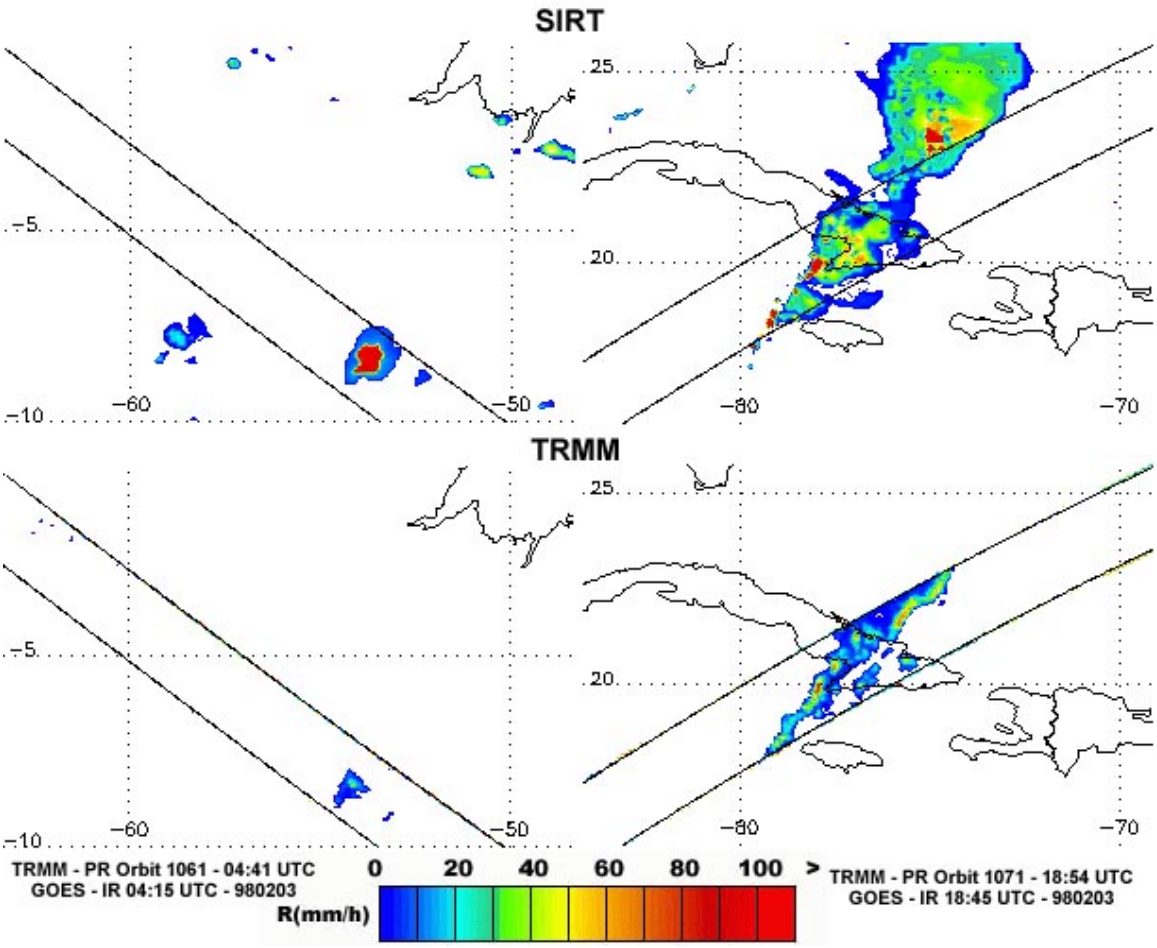

Figure 9: Instantaneous surface rainfall rates retrieved by SIRT (top panel) and TRMM-PR (bottom panel). Two storm cases are shown in this figure: (a) left, February 2nd 1998 at 04:15 UTC and TRMM orbit 1061; (b) right, February 2 nd 1998 at 18:45 UTC and TRMM orbit 1071.

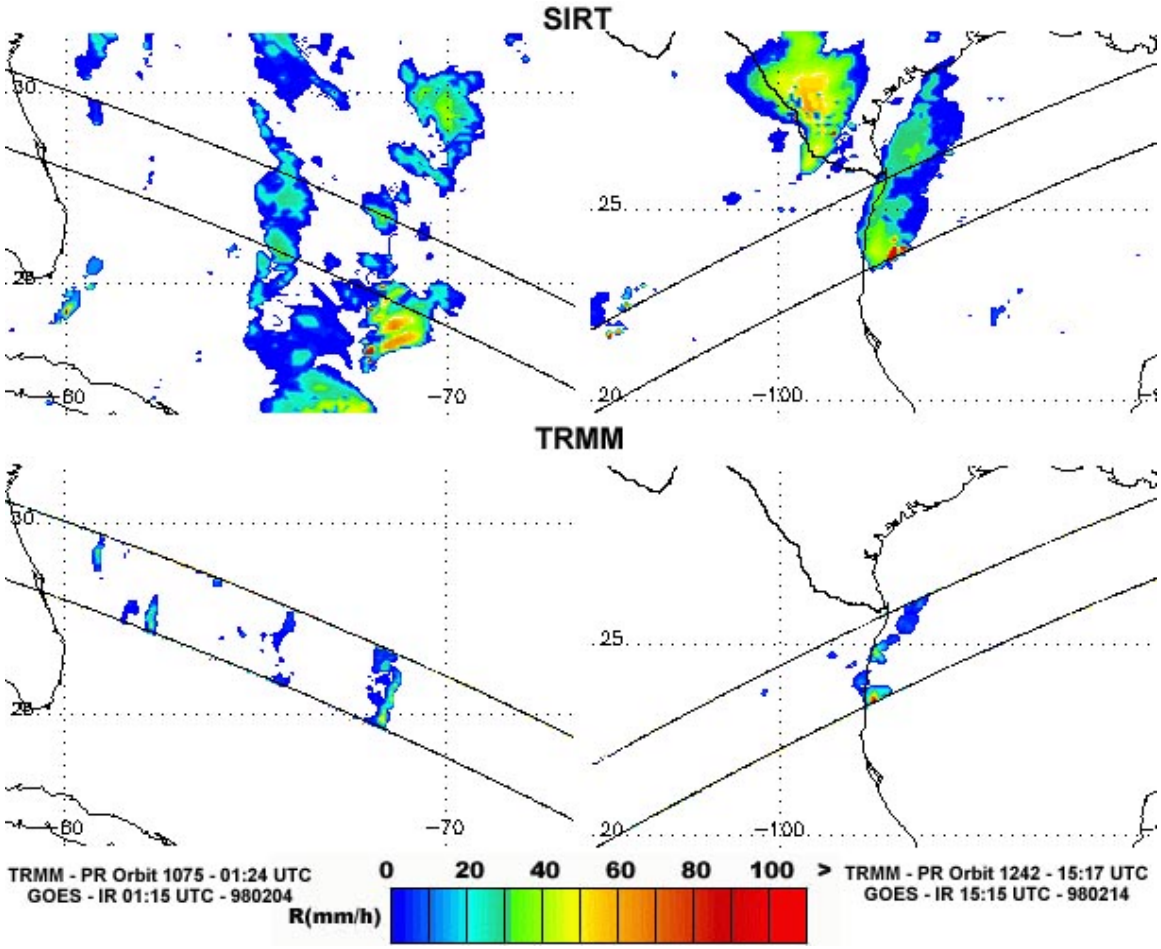

Figure 10: Instantaneous surface rainfall rates retrieved by SIRT (top panel) and TRMM-PR (bottom panel). Two storm cases are shown in this figure: (a) left, February 4th 1998 at 01:15 UTC and TRMM orbit 1075; (b) right, February 14 th 1998 at 15:15 UTC and TRMM orbit 1242.

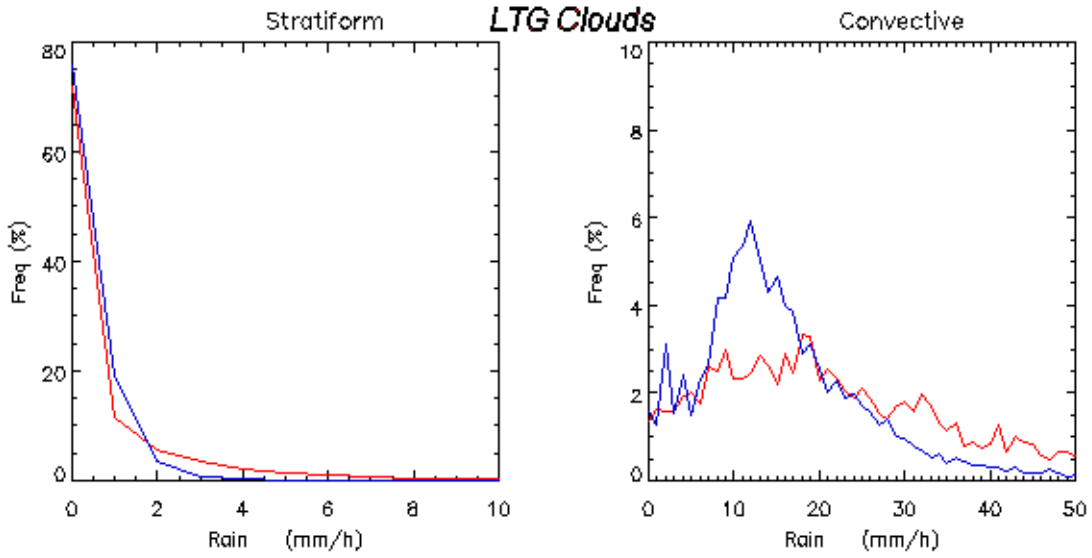

Figure 11: Stratiform (left panel) and convective (right panel) rainfall rates histograms for TRMM-PR (red line) and SIRT (blue line) for LTG clouds during February 1998.

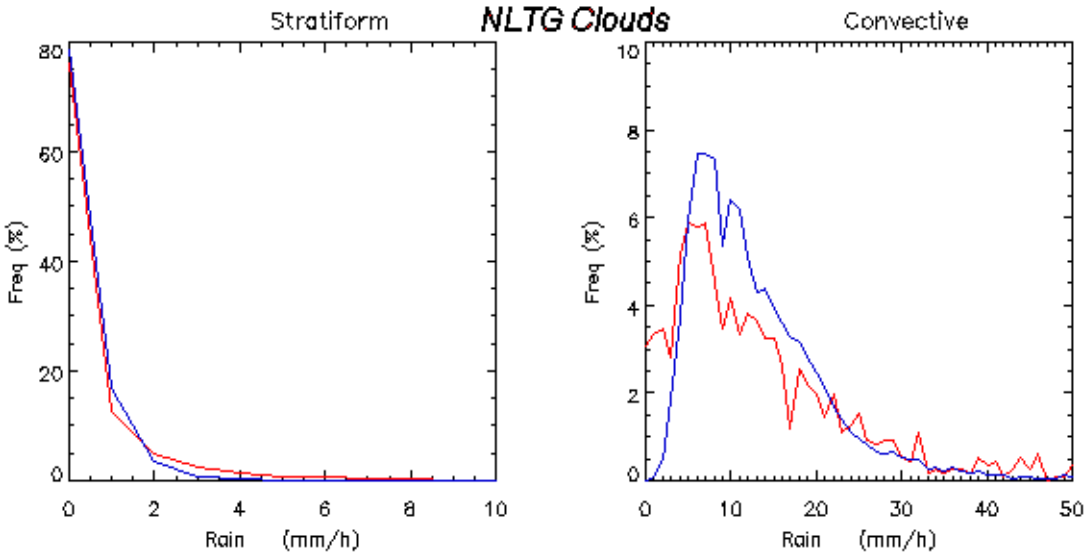

Figure 12: Same as in Figure 11 but for NLTG clouds during February 1998.

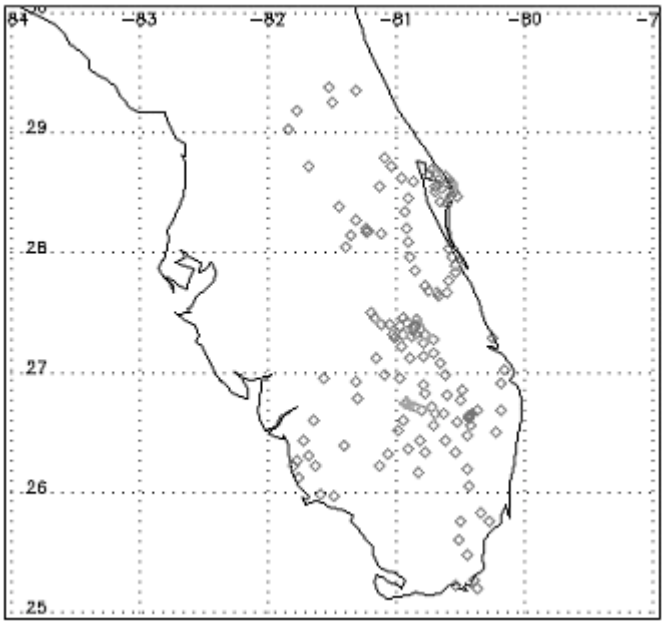

Figure 13: Configuration of the rain gauge network used in the study.

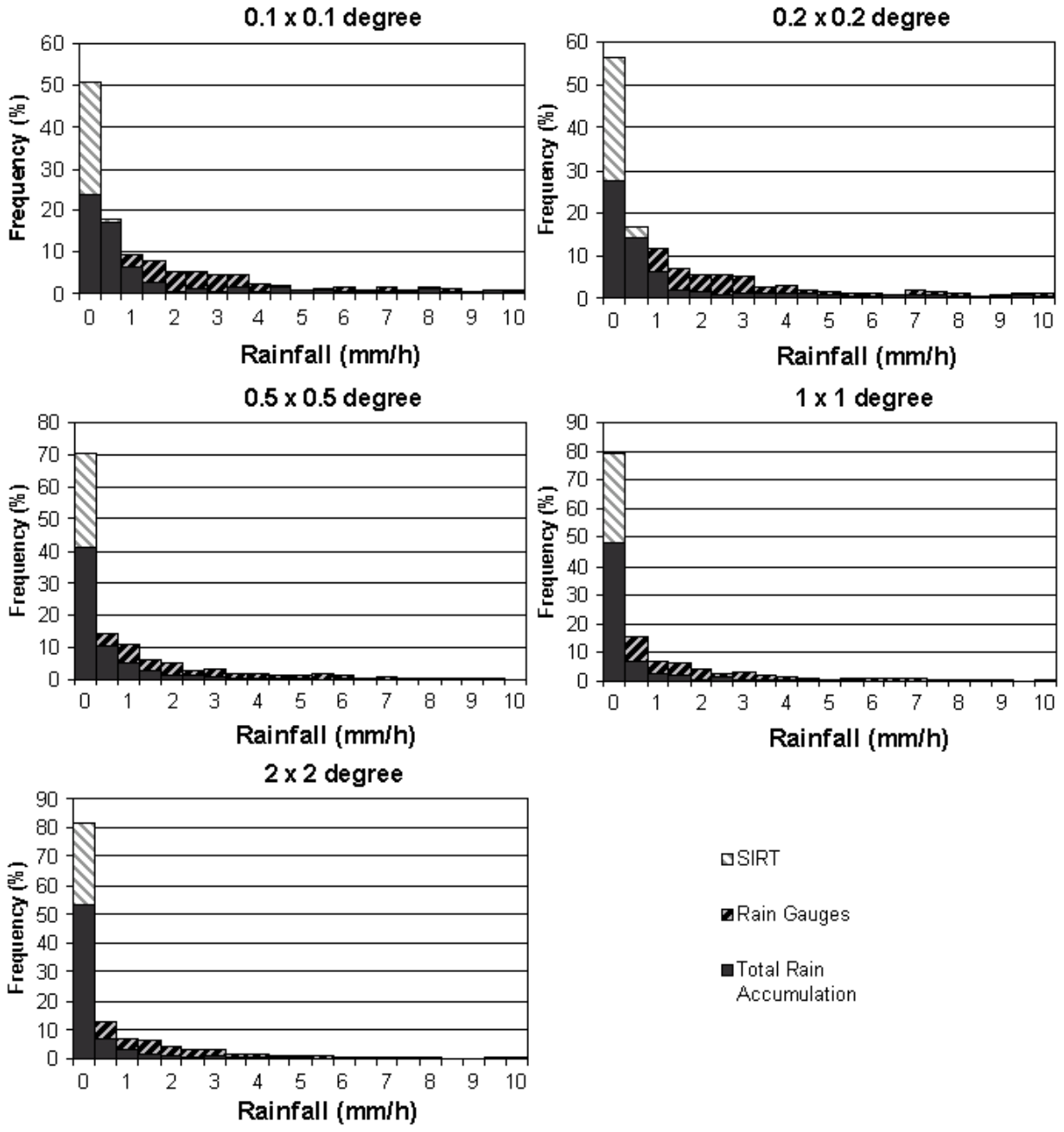

Figure 14: Hourly rainfall distributions derived from rain gauges (dark strips) and SIRT (white strips) for 0.1x0.1, 0.2x0.2, 0.5x0.5, 1x1, and 2x2 degree resolution. Solid dark gray bar represents common rainfall frequency observed by gauges and SIRT.